Learning Continuous Grasping Function with a Dexterous Hand from Human Demonstrations

Jianglong Ye*, Jiashun Wang*, Binghao Huang, Yuzhe Qin, Xiaolong Wang UC San Diego

Abstract: We propose to learn to generate grasping motion for manipulation with a dexterous hand using implicit functions. With continuous time inputs, the model can generate a continuous and smooth grasping plan. We name the proposed model Continuous Grasping Function (CGF). CGF is learned via generative modeling with a Conditional Variational Autoencoder using 3D human demonstrations. We will first convert the large-scale human-object interaction trajectories to robot demonstrations via motion retargeting, and then use these demonstrations to train CGF. During inference, we perform sampling with CGF to generate different grasping plans in the simulator and select the successful ones to transfer to the real robot. By training on diverse human data, our CGF allows generalization to manipulate multiple objects. Compared to previous planning algorithms, CGF is more efficient and achieves significant improvement on success rate when transferred to grasping with the real Allegro Hand. Our project page is at https://jianglongye.com/cgf.

Keywords: Dexterous Grasping, Implicit Function, Generative Model, Sim2Real

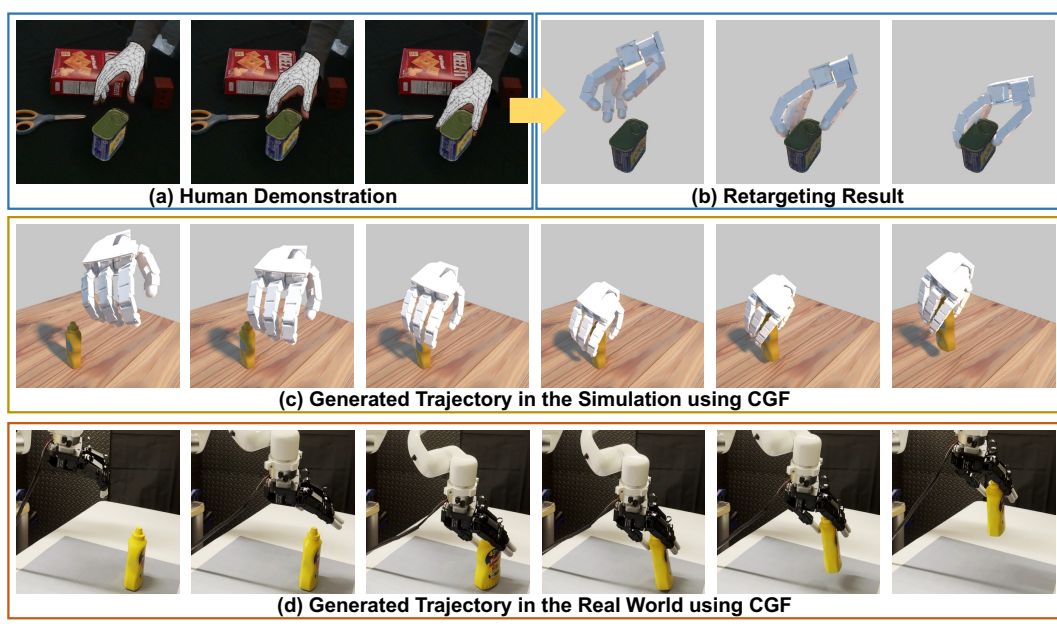


Figure 1: Examples of our generated trajectories learned from human demonstrations. Given hand-object trajectories from human video (a), we first translate them into robot manipulation demonstrations (b). We then train Continuous Grasping Function (CGF) to generate human-like trajectories and deploy them in simulation (c) and real robot (d).

^{*}equal contribution

1 Introduction

Learning to perform grasping with a multi-finger hand has been a long-standing problem in robotics [1, 2, 3, 4]. Using a dexterous hand instead of a parallel gripper offers the robot the flexibility on operating with daily life objects like humans do, but also largely increases the difficulty given the large Degree-of-Freedom of the dexterous hand. A typical method for this task is a 2-step paradigm including grasp pose estimations following by motion planning [5, 6, 7]. Recent works have also studied on using Reinforcement Learning with human demonstration guidance for grasping [8, 9].

While these approaches have shown encouraging results, they plan the grasping with finite discrete time steps. On the other hand, human grasping motion is continuous, can we learn a continuous grasping process for robot hands? Making robot grasping continuous can lead to a more natural and human-like trajectory, and each step we sample will be differentiable which we can use a more robust augmented PD controller. Recent progress on neural implicit functions have shown successful applications in learning continuous image representation [10, 11] and continuous 3D shape representation [12, 13, 14]. Can this success be migrated from representing 2D/3D space to time?

In this paper, we propose to learn Continuous Grasping Function (CGF) with a dexterous robotic hand. To mimic the continuous human motion, we utilize human grasp trajectories from videos to provide demonstrations and supervision in training. By training CGF with generative modeling on a large-scale of human demonstrations, it allows generalization to grasp multiple objects with a real Allegro robot hand as shown in Figure 1 (d).

Specifically, given the 3D hand-object trajectories from human videos (Figure 1 (a)), we first perform motion retargeting to convert the human hand motion to the robotic hand motion to obtain the robotic manipulation demonstrations (Figure 1 (b)). We then learn a CGF in the framework of a Conditional Variational AutoEncoder (CVAE) [15] by reconstructing the robotic hand motion with these demonstrations. Specifically, the conditional encoder of our CGF model will take the object point clouds as inputs and provides the object embedding. Taking the concatenation of the object embedding, a latent code z and a time parameter t, the decoder of CGF is an implicit function which outputs the dexterous hand parameters in the corresponding time t. By sampling a continuous-time sequence of t, we can recover a continuous grasping trajectory in any temporal resolution. By sampling the latent code z, we can achieve diverse trajectories for the same object. Figure 1 (c) shows an example of the inferred grasping trajectory in the simulator.

In our experiments on testing our model, we will perform sampling on the latent code z multiple times given a test object and generate diverse grasping trajectories. We then execute these trajectories in the simulator and select the one which can successfully grasp the object up. Different from the previous paradigm on grasping followed by planning, we empirically find our method is much more efficient since we avoid performing planning for each trajectory but directly generate the trajectory from CGF. Given the selected trajectories from the simulator, we can deploy them in the real world with an Allegro hand attached on an X-Arm 6 robot. Compared with planning, our method achieves better Sim2Real generalization with more natural and human-like motion, which leads to a better success rate.

We highlight our main contributions here: (i) A novel Continuous Grasping Function (CGF) model which allows smooth and dense sampling in time for generating grasping trajectory; (ii) CGF allows efficient generation of grasping plan and more robust control in simulation; (iii) We achieve much significant improvement on Sim2Real generation on Allegro hand by learning CGF from human demonstrations.

2 Related Work

Generalization in Dexterous Manipulation. Dexterous manipulation is one of the most challenging problems in robotics [1, 2, 3, 4, 16, 17, 18]. Recent studies on model-free [19, 20, 21, 22] and model-based [23, 24] Reinforcement Learning (RL) have achieved encouraging results on multiple complex dexterous manipulation tasks. However, there is still a large challenge on generalization for RL. For example, when the RL policy in [19] can be transferred to the real robot, it is learned specifically for one object. On the other hand, an RL policy trained with multiple objects in simulator [22] has not yet been transferred to real. Instead of using RL, one line of works on dexterous grasping is first performing a grasp estimation and then planning for execution [25, 26, 5, 7], which

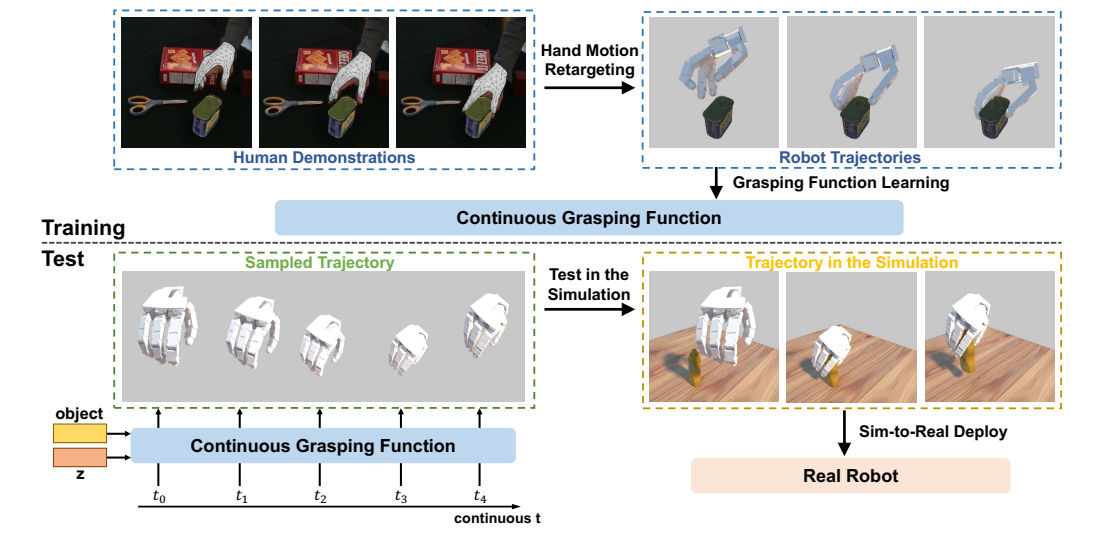


Figure 2: Pipeline overview. During training, human demonstrations are first translated to robot joint positions which serve as the supervision for grasping function learning. During inference, our trained CGF takes a sampled latent code z, object feature and query time sequence as inputs to generate the trajectory. We then execute these trajectories in the simulator and deploy successful ones to the real robot.

have shown great success on generalization to multiple objects and in real robot at the same time. Our work is more close to this line of research, where we achieve generalization by learning a continuous grasping function from human videos. Different from previous works, our method allows more smooth and natural grasping generation and it is also more efficient and accurate at the same time. We will provide comparisons to previous planning approaches in our experiments.

Grasping Motion Synthesis. Synthesizing and predicting human grasp has been an active research field for both computer vision and robotics [6, 27, 28, 29, 30, 31]. For example, Grasping Field [28] is proposed as an implicit function that generates plausible human grasps given a 3D object. However, to apply on the robot hand, we will need to synthesize the full motion instead of a static pose. This motivates the research on synthesizing the hand-object interaction motions [32, 33, 34, 35, 36, 37]. For example, a full body and hand motion are synthesized together to grasp an object in [34]. While related to our work, most approaches are still focusing on modeling the human hand. In this paper, we provide a framework where we first retarget the human hand trajectories to the robot hand trajectories and learn the robot grasping function with them.

Learning from Human Demonstrations. Our work is related to imitation learning or RL with human demonstrations for not only parallel grippers [38, 39, 40] but also dexterous hands [41, 42, 43, 44, 45, 9, 46, 47, 48]. For example, DexMV is a platform proposed in [9] for extracting 3D human demonstrations from videos, generating robot demonstrations by retargeting, and augmenting Reinforcement Learning with these demonstrations for multiple manipulation tasks. While we both share similar methods on obtaining robot demonstrations for training, the RL approach taken GT states as inputs in DexMV limits its generalizability to multiple objects and real robot transfer. On the other hand, our implicit function is able to generate continuous grasping given a point cloud input and it can be deployed in the real robot. As most RL approaches are still with full access to GT states, they are not directly comparable to our method.

Implicit Functions for Robotic Tasks. Beyond its successful applications in computer vision, implicit functions have recently been explored in robotic manipulation tasks [49, 50, 51, 52, 53]. For example, NeRF [14] is used as a manner for learning 3D representations for control in [49]. Instead of using implicit functions to learn static 3D representations, our work focuses on the continuity in time. We build a grasping function to directly generate the trajectory instead of a static scene.

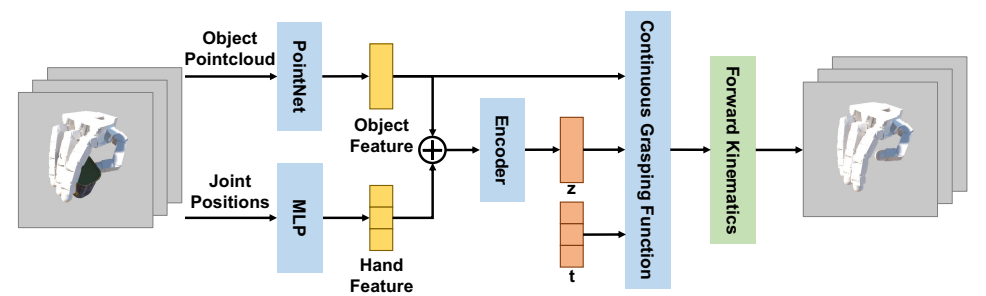


Figure 3: Network architecture. Our generative model takes object point cloud and a sequence of joint positions as input and recovers corresponding robot hands. The proposed CGF takes the latent code z, object feature, and the query time t as inputs to predict the corresponding joint position q_t . \oplus denotes concatenation.

3 Method

3.1 Overview

We aim to learn human-like robot grasping given object point clouds as input. We emphasize that learning from human demonstration could lead to more natural trajectories and continuity helps the following control. To this end, we train Continuous Grasping Function in the CVAE framework to generate continuous trajectories and deploy them in the simulator and real robot consecutively. The pipeline is shown in Fig. 2. During training, we first perform hand motion retargeting on a large-scale hand-object interaction dataset [54] to collect demonstrations. Then the retargeting results are used as the supervision for the grasping function learning. During inference, numerous continuous trajectories are sampled for a specific object and tested in the simulator. The successful trajectory will be deployed to the real robot. Besides, we can take more advantage of continuous implicit function by utilizing augmented PD control with the derivative of the joint positions.

3.2 Human Demonstration Translation

The data collection of human hand-object interaction is relatively well developed and more convenient. Using large-scale human hand-object interaction data, we can learn the pattern of how dexterous hands manipulate the object and we hope to generalize it to the robot hand. And in this paper, we use ground truth trajectories from DexYCB [54]. Translating human hand motion to robotics motion is the first step. Following [47], we formulate our hand motion retargeting problem as a position-based optimization problem. We encourage the robot's keypoint position to be as close as possible to its corresponding human hand joint position,

$$\min_{q_t} \sum_{i=0}^{N} ||\mathcal{J}_i(q_t) - j_i||^2 + \lambda ||\mathcal{J}_i(q_t) - \mathcal{J}_i(q_{t-1})||^2 \quad \text{s.t. } q_{lower} \le q_t \le q_{upper}, \quad (1)$$

where q_t is joint position at time t, \mathcal{J}_i is the forward kinematics function of the i-th joint and j_i is the Cartesian coordinates of the hand joint which matches the i-th joint of the robot. q_{lower} and q_{upper} are the joint limits. We also ensure smoothness by adding a normalization term to penalize a large distance between q_t and q_{t-1} . We set the initial $q_0 = \frac{1}{2}(q_{lower} + q_{upper})$.

3.3 Continuous Grasping Function Learning

Our generative model is based on Conditional Variational Auto-Encoder (CVAE) [55], where we propose Continuous Grasping Function (CGF) to replace the traditional decoder. During training, both encoder and CGF are used to learn the grasping generation in a robot hand reconstruction task with object point clouds and robot joint positions as inputs; During inference, only CGF is used to generate continuous grasping with only objects as input. The architecture is shown in Figure 3.

During training, given the object point cloud $\mathcal{P}^o \in \mathbb{R}^{N \times 3}$ (N is the number of points) and a sequence of joints positions $\{q_t\}, t \in \{0, 1, \cdots, T\}$ (T is the number of frames) as inputs, we utilize PointNet [56] and MLP to extract object feature $\mathcal{F}^o \in \mathbb{R}^{1024}$ and hand features $\{\mathcal{F}^h_t\} \in \mathbb{R}^{256}$ respectively. All these features are then concatenated as \mathcal{F}^{oh} for the encoder input. The outputs of the encoder are the mean $\mu \in \mathbb{R}^{256}$ and variance $\sigma^2 \in \mathbb{R}^{256}$ of the Gaussian distribution $\mathcal{Q}\left(z \mid \mu, \sigma^2\right)$. The latent code z is sampled from the distribution for the hand reconstruction.

After the encoding and sampling, we use our CGF to decode a continuous grasping. Inspired by implicit functions [12, 13, 57] for shape representation, our proposed CGF maps the query time t to the joint position q_t . Similar to the traditional CVAE, we also concatenate latent code z and the object feature \mathcal{F}^o with time t as the input for CGF. Specifically, CGF is a MLP f parameterized by θ which predicts the corresponding joint position \hat{q}_t :

$$\hat{q}_t = f(t, z, \mathcal{F}^o; \theta). \tag{2}$$

We reverse the time and define t=0 as the end of the grasping, i.e., when the robot's hand touches the object. And as t grows, the hand moves further away from the object. Given the predicted joint position \hat{q}_t , a differentiable forward kinematics layer \mathcal{J}_i is utilized to get the Cartesian coordinate of the i-th joint.

The first objective function is the reconstruction error, which is defined as the $\mathcal{L}2$ distance between the joint positions as well as their Cartesian coordinates. We denote them as $\mathcal{L}_q = \sum_{t=0}^{T-1} \|\hat{q}_t - q_t\|_2^2$ and $\mathcal{L}_j = \sum_{t=0}^{T-1} \sum_{i=0} \|\mathcal{J}_i(\hat{q}_t) - \mathcal{J}_i(q_t)\|_2^2$ respectively. Following the training of VAE [25], we define a KL loss to encourage the latent code distribution $\mathcal{Q}\left(z\mid\mu,\sigma^2\right)$ to be close to the standard Gaussian distribution, which is achieved by maximazing the KL-Divergence as $\mathcal{L}_{KL} = -D_{KL}\left(Q\left(z\mid\mu,\sigma^2\right)\|\mathcal{N}(0,I)\right)$. We also introduce a contact loss at the end of the grasping to push the tips of robot hand to the object surface, which is achieved by minimizing distances to their closest object points $\mathcal{L}_{contact} = \sum_i \min_{p \in \mathcal{P}^o} \|\mathcal{J}_i(q_0) - p\|_2^2$ where i belongs to the indices of all tips. The full training loss is:

$$\mathcal{L} = \lambda_q \mathcal{L}_q + \lambda_j \mathcal{L}_j + \lambda_{KL} \mathcal{L}_{KL} + \lambda_c \mathcal{L}_{contact}, \tag{3}$$

where $\lambda_a, \lambda_i, \lambda_{KL}$ and λ_c are weights for various losses.

During inference, our CGF can easily sample diverse trajectories. We use the PointNet to get the object feature \mathcal{F}^o and sample a random latent code z from a Gaussian distribution, then with a time query sequence, our CGF can produce a continuous and natural trajectory.

3.4 Augmented PD Control

Different from previous works, we use an implicit function to output the target joint position q_d , and given the property of the implicit function, we can easily get the derivative (target joint velocity) \dot{q}_d and the second-order derivative (target joint acceleration) \ddot{q}_d . Thus we can use a more robust controller, augmented PD control with the form of

$$\tau = \text{ID}(\ddot{q}_d, q, \dot{q}) - K_p e - K_v \dot{e}, \tag{4}$$

where $e=q-q_d$, $\dot{e}=\dot{q}-\dot{q}_d$, τ is the joint torque and $\mathrm{ID}(\ddot{q}_d,q,\dot{q})$ is the inverse dynamics. K_p and K_v are hyperparameters. q, \dot{q} and \ddot{q} are the joint position, velocity and acceleration of the robot. As far as we know, our method is the first end-to-end manner that can directly get the derivative to use the augmented PD control.

4 Experiments

We perform qualitative and quantitative evaluations of the grasping generated by our method. We show that by learning from human demonstrations, our method is more efficient in finding successful grasping in the simulator. We do not plan for each trajectory, instead, we sample a large number of trajectories to get successful trajectories.

We conduct real-world experiments for the successful trajectories using an Allegro hand attached on X-Arm 6, which shows that our generation results have the ability to be transferred to the real robot with a higher success rate.

4.1 Experimental Setting

Datasets. We utilize the DexYCB dataset [54] for the human demonstrations. DexYCB contains 1,000 sequences of human grasping motions with 20 YCB objects [58]. We use 15 of them as training objects and 5 of them as test objects. We filter out all left-handed sequences and perform hand motion retargeting on the other sequences to translate the hand motion into allegro robot motion.

Baselines. For a fair comparison, we employ GraspTTA [29], which is also based on a generative model, to synthesize the grasp pose. We apply the same hand motion retargeting to the GraspTTA

	Smoothness - Joints		Smoothness - Cartesian			
Method	Pos ↓	$\text{Vel (log)} \downarrow$	$Acc\ (log) \downarrow$	Pos ↓	Vel (log) \downarrow	Acc (log) \downarrow
GraspTTA [29] + RRT	3.19	3.40	6.43	7.82	3.80	6.83
GraspTTA [29] + CEM-MPC	6.96	3.09	5.50	13.18	3.33	5.74
Ours	9.77	2.03	3.47	5.39	1.84	3.31
Linear Interpolation	1.00	-3.58	-1.99	1.96	0.70	1.38

Table 1: Smoothness evaluation. For smoothness of joint positions and Cartesian coordinates, our CGF outperforms baselines by a large margin, which helps produce more natural trajectories and better control.

to get the final joint positions. And we utilize rapidly exploring random tree (RRT) [59] and cross-entropy method (CEM) [60] with model predictive control (MPC) [61] for planning the trajectory to reach the grasp pose. We name them GraspTTA+RRT and GraspTTA+CEM-MPC respectively. Note that GraspTTA+CEM-MPC is used for generating the demonstrations in [48]. And we use its reward for CEM-MPC. In addition, we perform linear interpolation between the beginning and ending joint positions generated by our method and take it as a trivial baseline.

Implementation Details. For training CGF, we sample 2,000 points on the object mesh as the input object point clouds. During training, we employ the Adam optimizer with the learning rate 5e-4, where the learning rate is reduced by half per 500 epochs. The batch size is 32. The training takes 1000 epochs in total. The loss weights are $\lambda_q=1$, $\lambda_j=10$, $\lambda_{KL}=1e-3$ and $\lambda_c=50$. We sample 10,000 latent codes for CGF and output the trajectories. For simulation experiments, environments are built upon the Sapien [62] simulator.

For baselines, we use GraspTTA to generate 200 grasp poses for each object. For RRT, we set 10,000 nodes in the tree, and set step size $\epsilon=0.01$ and probability of sampling $\beta=0.5$. For CEM-MPC, we set popsize M=100, time horizon T=5, number of elites e=10, and iterations I=2.

4.2 Evaluation Metrics

Smoothness. To evaluate the continuity of the generated grasping, we propose to compare the smoothness. We first normalize joint positions by making all joints start at 0 and end at 1 in all trajectories. Then we calculate discrete first-order and second-order gradients, i.e. velocity and acceleration. Smoothness is defined as the sum of the $\mathcal{L}1$ distances of position, velocity, and acceleration between neighboring frames. Note that the linear interpolation is upper bound with a joint position smoothness of 1.0.

Cost per successful trajectory in the simulator. Though planning-based methods could improve the success possibilities for each trajectory but the cost of such planning should not be ignored. We argue some times what we want is just successful trajectories. At this point, it is important to evaluate the average cost of one successful trajectory. Thus we perform evaluations on this average cost among baselines and our method in the simulator. Our method and GraspTTA+CEM-MPC require environment step during the planning, the cost is how many steps per successful trajectory. And GraspTTA+RRT requires collision checks during the planning. So the cost is how many collision checks per successful trajectory.

Success rate in real-world. We also evaluate the success rate in the real world. Note the successful trajectories in the simulator do not guarantee success in the real world because of the sim-to-real gap. For our method and all the baselines, we pick the successful trajectories and deploy them in the real world and count the success rate in the real world. This reflects the sim-to-real transfer ability.

4.3 Simulated Experimental Results

Smoothness evaluation. We compare the smoothness with three baselines and summarize the results in Tab. 1. For better comparison, the smoothness for velocity and acceleration is in the log form. For both joint positions and Cartesian coordinates, our CGF outperforms baselines by a large margin. Note that for the joint position smoothness, our method does not show an advantage over the baseline. This is due to that humans tend to follow a natural curve rather than the shortest path. Nevertheless, the improvement in the smoothness of velocity and acceleration plays an important role in producing natural trajectories and better control.

Success cost evaluation. The average cost per successful trajectory is in Tab. 2. For better comparison, the number of simulation steps and collision detection is in the log form. Since we directly

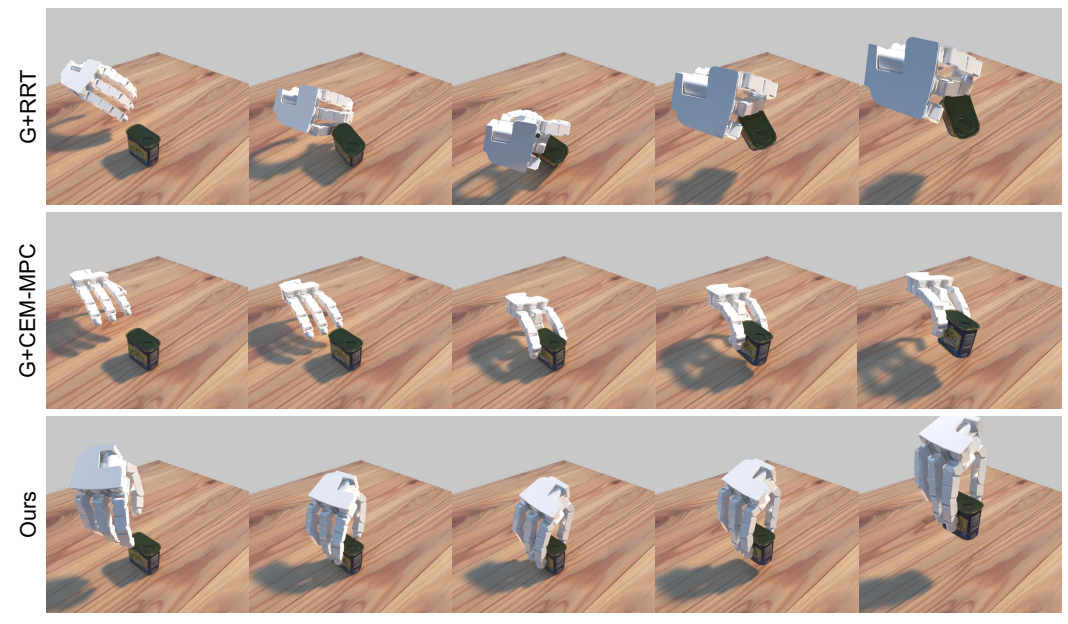


Figure 4: Qualitative evaluation in the simulation. Because of human demonstrations, our CGF generates a more natural and reasonable trajectory, which is helpful for the sim-to-real transfer. G is short for GraspTTA.

	Cost / Successful Trajectory (log) ↓		
Method	Seen Object	Unseen Object	
GraspTTA [29] + RRT	5.41*	5.55*	
GraspTTA [29] + CEM-MPC	5.96	6.16	
Ours	4.29	4.67	
Linear Interpolation	-	-	

Table 2: Success cost evaluation. Since our method only requires a few simulation steps to test a trajectory, the average cost for a successful trajectory is much lower than baselines. Note that we calculate the amount of collision detection for RRT.

execute the target joint positions generated from our CGF, through sampling a large number of trajectories, we can get a certain number of successful trajectories. Quantitatively, the average cost of getting a successful trajectory is significantly lower than the GraspTTA+RRT and GraspTTA+CEM-MPC, which both require a large cost. We also evaluate the cost of unseen objects, although the cost increased a little, our method still surpasses the baselines. Although the linear interpolation produces the smoothest trajectory, it never grasps an object successfully in the simulator.

Qualitative evaluation. We visualize the typical trajectories of the baselines and our method in Fig. 4. Since RRT is only planning the reachable target joint positions, the trajectory may not be natural. And a small perturbation in the execution process may cause it to collide with objects. CEM-MPC is not a long-time horizon method, which will make it fall into a local optimum very quickly. As shown in Fig. 4, the middle finger is not in the ideal position. However, our CGF, learning from the human demonstration, could generate a much more natural and smooth trajectory. This is helpful for the sim-to-real transfer, which we will discuss in the next section.

4.4 Real-World Robot Experiments

Setup. For the real-world robot experiments, we attached an Allegro hand on an X-Arm 6 robot. We use 3 real objects from YCB [58] which are *Mustard Bottle*, *Tomato Soup Can* and *Potted Meat Can*. We assume the pose of the object is given and use open-loop control for grasping.

Results with a Real Robot Hand. We test the sim-to-real transfer ability of the trajectories generated by our method and baselines. For each object and method, we sample 20 successful trajectories in the simulator to deploy in the real world. We report the success rate in Tab. 3. Although all the trajectories succeeded in the simulator, our method has a much higher success rate in the real world than the baselines. Since our method is learning from human demonstration, it is beneficial for natural trajectory generation. And the use of implicit function could help to provide a continuous and

	Success Rate (%) ↑			Cost / Succ. Traj. (log) ↓			
Method	Meat Can	Soup Can	Bottle	Meat Can	Soup Can	Bottle	
GraspTTA [29] + RRT	10.0	5.0	5.0	6.41	6.72	6.72	
GraspTTA [29] + CEM-MPC	15.0	5.0	0.0	6.78	7.26	-	
Ours	30.0	40.0	35.0	4.81	4.69	4.74	

Table 3: Real-world experiments. For the successful trajectories in the simulation, our CGF has a higher success rate in the real world.

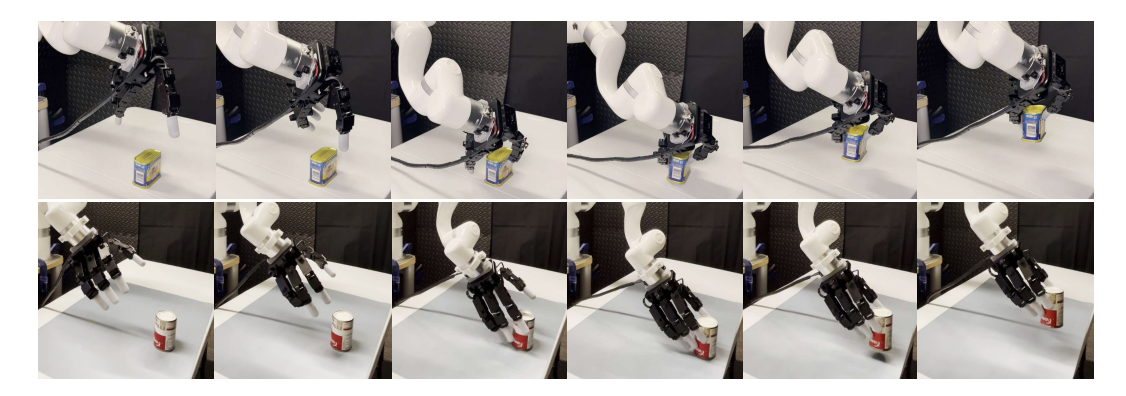


Figure 5: Real-world results on *Potted Meat Can* and *Tomato Soup Can*. Our CGF successfully transfers the simulation trajectory to the real robot.

more smooth trajectory. We believe these are crucial factors to improve the sim-to-real transfer ability. At the same time, in order to get successful trajectories in the real world, generating trajectories by our CGF is a more efficient way compared to traditional planning methods as Tab. 3 shows. We further provide a visualization of our successful trajectories in the real world in Fig. 5. Our method could generate natural and human-like grasping.

5 Conclusion and Limitation

Conclusion. We propose a novel implicit function named Continuous Grasping Function to generate smooth and dense grasping trajectories. CGF is learned in the framework of a Conditional Variational AutoEncoder using 3D human demonstrations. During inference, we sample various grasping plans in the simulator and deploy the successful ones to the real robot. By training on diverse human-object data, our method allows generalization to manipulate multiple objects. Compared to previous planning algorithms, CGF is more efficient and has a better sim-to-real generalization ability.

Limitation. There are mainly two limitations for our approach: (i) Similar to other 2-step approaches with grasp estimation followed by motion planning, our method is open-loop and the interaction feedback is not applied to adjust grasping; (ii) 6D object pose estimation is required for both simulation and the real robot.

References

- [1] J. K. Salisbury and J. J. Craig. Articulated hands: Force control and kinematic issues. *The International journal of Robotics research*, 1(1):4–17, 1982.
- [2] D. Rus. In-hand dexterous manipulation of piecewise-smooth 3-d objects. *The International Journal of Robotics Research*, 1999.
- [3] A. M. Okamura, N. Smaby, and M. R. Cutkosky. An overview of dexterous manipulation. In *ICRA*, 2000.
- [4] M. R. Dogar and S. S. Srinivasa. Push-grasping with dexterous hands: Mechanics and a method. 2010.
- [5] J. Varley, J. Weisz, J. Weiss, and P. Allen. Generating multi-fingered robotic grasps via deep learning. In 2015 IEEE/RSJ international conference on intelligent robots and systems (IROS), pages 4415–4420. IEEE, 2015.
- [6] S. Brahmbhatt, A. Handa, J. Hays, and D. Fox. Contactgrasp: Functional multi-finger grasp synthesis from contact. In 2019 IEEE/RSJ International Conference on Intelligent Robots and Systems (IROS), pages 2386–2393. IEEE, 2019.
- [7] Q. Lu, K. Chenna, B. Sundaralingam, and T. Hermans. Planning multi-fingered grasps as probabilistic inference in a learned deep network. In *Robotics Research*, pages 455–472. Springer, 2020.
- [8] P. Mandikal and K. Grauman. Learning dexterous grasping with object-centric visual affordances. In 2021 IEEE International Conference on Robotics and Automation (ICRA), pages 6169–6176. IEEE, 2021.
- [9] Y. Qin, Y.-H. Wu, S. Liu, H. Jiang, R. Yang, Y. Fu, and X. Wang. Dexmv: Imitation learning for dexterous manipulation from human videos. *arXiv* preprint arXiv:2108.05877, 2021.
- [10] Y. Chen, S. Liu, and X. Wang. Learning continuous image representation with local implicit image function. In *Proceedings of the IEEE/CVF conference on computer vision and pattern recognition*, pages 8628–8638, 2021.
- [11] E. Dupont, Y. W. Teh, and A. Doucet. Generative models as distributions of functions. *arXiv* preprint arXiv:2102.04776, 2021.
- [12] J. J. Park, P. Florence, J. Straub, R. Newcombe, and S. Lovegrove. Deepsdf: Learning continuous signed distance functions for shape representation. In *Proceedings of the IEEE/CVF conference on computer vision and pattern recognition*, pages 165–174, 2019.
- [13] L. Mescheder, M. Oechsle, M. Niemeyer, S. Nowozin, and A. Geiger. Occupancy networks: Learning 3d reconstruction in function space. In *Proceedings of the IEEE/CVF conference on computer vision and pattern recognition*, pages 4460–4470, 2019.
- [14] B. Mildenhall, P. P. Srinivasan, M. Tancik, J. T. Barron, R. Ramamoorthi, and R. Ng. Nerf: Representing scenes as neural radiance fields for view synthesis. In *European conference on computer vision*, pages 405–421. Springer, 2020.
- [15] K. Sohn, H. Lee, and X. Yan. Learning structured output representation using deep conditional generative models. In NIPS, 2015.
- [16] N. C. Dafle, A. Rodriguez, R. Paolini, B. Tang, S. S. Srinivasa, M. Erdmann, M. T. Mason, I. Lundberg, H. Staab, and T. Fuhlbrigge. Extrinsic dexterity: In-hand manipulation with external forces. In 2014 IEEE International Conference on Robotics and Automation (ICRA), pages 1578–1585. IEEE, 2014.
- [17] Y. Bai and C. K. Liu. Dexterous manipulation using both palm and fingers. 2014.
- [18] B. Calli, A. Kimmel, K. Hang, K. Bekris, and A. Dollar. Path planning for within-hand manipulation over learned representations of safe states. In *International Symposium on Experimental Robotics*, pages 437–447. Springer, 2018.

- [19] OpenAI, M. Andrychowicz, B. Baker, M. Chociej, R. Józefowicz, B. McGrew, J. Pachocki, A. Petron, M. Plappert, G. Powell, A. Ray, J. Schneider, S. Sidor, J. Tobin, P. Welinder, L. Weng, and W. Zaremba. Learning dexterous in-hand manipulation. *arXiv*, 2018.
- [20] OpenAI, I. Akkaya, M. Andrychowicz, M. Chociej, M. Litwin, B. McGrew, A. Petron, A. Paino, M. Plappert, G. Powell, R. Ribas, J. Schneider, N. Tezak, J. Tworek, P. Welinder, L. Weng, Q. Yuan, W. Zaremba, and L. Zhang. Solving rubik's cube with a robot hand. *arXiv*, 2019.
- [21] W. Huang, I. Mordatch, P. Abbeel, and D. Pathak. Generalization in dexterous manipulation via geometry-aware multi-task learning. *arXiv preprint arXiv:2111.03062*, 2021.
- [22] T. Chen, J. Xu, and P. Agrawal. A system for general in-hand object re-orientation. In *Conference on Robot Learning*, pages 297–307. PMLR, 2022.
- [23] V. Kumar, E. Todorov, and S. Levine. Optimal control with learned local models: Application to dexterous manipulation. In 2016 IEEE International Conference on Robotics and Automation (ICRA), pages 378–383. IEEE, 2016.
- [24] A. Nagabandi, K. Konolige, S. Levine, and V. Kumar. Deep dynamics models for learning dexterous manipulation. In *Conference on Robot Learning*, pages 1101–1112. PMLR, 2020.
- [25] S. Andrews and P. G. Kry. Goal directed multi-finger manipulation: Control policies and analysis. *Computers & Graphics*, 2013.
- [26] D. Kappler, J. Bohg, and S. Schaal. Leveraging big data for grasp planning. In 2015 IEEE International Conference on Robotics and Automation (ICRA), pages 4304–4311. IEEE, 2015.
- [27] O. Taheri, N. Ghorbani, M. J. Black, and D. Tzionas. Grab: A dataset of whole-body human grasping of objects. In *European conference on computer vision*, pages 581–600. Springer, 2020.
- [28] K. Karunratanakul, J. Yang, Y. Zhang, M. J. Black, K. Muandet, and S. Tang. Grasping field: Learning implicit representations for human grasps. In *2020 International Conference on 3D Vision (3DV)*, pages 333–344. IEEE, 2020.
- [29] H. Jiang, S. Liu, J. Wang, and X. Wang. Hand-object contact consistency reasoning for human grasps generation. In *Proceedings of the IEEE/CVF International Conference on Computer Vision*, pages 11107–11116, 2021.
- [30] P. Grady, C. Tang, C. D. Twigg, M. Vo, S. Brahmbhatt, and C. C. Kemp. Contactopt: Optimizing contact to improve grasps. In *Proceedings of the IEEE/CVF Conference on Computer Vision and Pattern Recognition*, pages 1471–1481, 2021.
- [31] L. Yang, X. Zhan, K. Li, W. Xu, J. Li, and C. Lu. Cpf: Learning a contact potential field to model the hand-object interaction. In *Proceedings of the IEEE/CVF International Conference on Computer Vision*, pages 11097–11106, 2021.
- [32] K. Hsiao and T. Lozano-Perez. Imitation learning of whole-body grasps. In 2006 IEEE/RSJ international conference on intelligent robots and systems, pages 5657–5662. IEEE, 2006.
- [33] Y. Ye and C. K. Liu. Synthesis of detailed hand manipulations using contact sampling. *ACM Transactions on Graphics (TOG)*, 31(4):1–10, 2012.
- [34] Y. Wu, J. Wang, Y. Zhang, S. Zhang, O. Hilliges, F. Yu, and S. Tang. Saga: Stochastic whole-body grasping with contact. *arXiv preprint arXiv:2112.10103*, 2021.
- [35] H. Zhang, Y. Ye, T. Shiratori, and T. Komura. Manipnet: neural manipulation synthesis with a hand-object spatial representation. *ACM Transactions on Graphics (TOG)*, 40(4):1–14, 2021.
- [36] O. Taheri, V. Choutas, M. J. Black, and D. Tzionas. Goal: Generating 4d whole-body motion for hand-object grasping. In *Proceedings of the IEEE/CVF Conference on Computer Vision and Pattern Recognition*, pages 13263–13273, 2022.

- [37] S. Christen, M. Kocabas, E. Aksan, J. Hwangbo, J. Song, and O. Hilliges. D-grasp: Physically plausible dynamic grasp synthesis for hand-object interactions. In *Proceedings of the IEEE/CVF Conference on Computer Vision and Pattern Recognition*, pages 20577–20586, 2022.
- [38] K. Schmeckpeper, O. Rybkin, K. Daniilidis, S. Levine, and C. Finn. Reinforcement learning with videos: Combining offline observations with interaction. *arXiv*, 2020.
- [39] L. Shao, T. Migimatsu, Q. Zhang, K. Yang, and J. Bohg. Concept2robot: Learning manipulation concepts from instructions and human demonstrations. In RSS, 2020.
- [40] S. Young, D. Gandhi, S. Tulsiani, A. Gupta, P. Abbeel, and L. Pinto. Visual imitation made easy. arXiv, 2020.
- [41] A. Gupta, C. Eppner, S. Levine, and P. Abbeel. Learning dexterous manipulation for a soft robotic hand from human demonstrations. In 2016 IEEE/RSJ International Conference on Intelligent Robots and Systems (IROS), pages 3786–3793. IEEE, 2016.
- [42] V. Kumar, A. Gupta, E. Todorov, and S. Levine. Learning dexterous manipulation policies from experience and imitation. *arXiv* preprint arXiv:1611.05095, 2016.
- [43] A. Rajeswaran, V. Kumar, A. Gupta, G. Vezzani, J. Schulman, E. Todorov, and S. Levine. Learning complex dexterous manipulation with deep reinforcement learning and demonstrations. arXiv preprint arXiv:1709.10087, 2017.
- [44] S. Christen, S. Stevšić, and O. Hilliges. Guided deep reinforcement learning of control policies for dexterous human-robot interaction. In 2019 International Conference on Robotics and Automation (ICRA), pages 2161–2167. IEEE, 2019.
- [45] G. Garcia-Hernando, E. Johns, and T.-K. Kim. Physics-based dexterous manipulations with estimated hand poses and residual reinforcement learning. In 2020 IEEE/RSJ International Conference on Intelligent Robots and Systems (IROS), pages 9561–9568. IEEE, 2020.
- [46] A. Sivakumar, K. Shaw, and D. Pathak. Robotic telekinesis: learning a robotic hand imitator by watching humans on youtube. *arXiv preprint arXiv:2202.10448*, 2022.
- [47] Y. Qin, H. Su, and X. Wang. From one hand to multiple hands: Imitation learning for dexterous manipulation from single-camera teleoperation. *arXiv preprint arXiv:2204.12490*, 2022.
- [48] Y.-H. Wu, J. Wang, and X. Wang. Learning generalizable dexterous manipulation from human grasp affordance. *arXiv preprint arXiv:2204.02320*, 2022.
- [49] X. Li, S. De Mello, X. Wang, M.-H. Yang, J. Kautz, and S. Liu. Learning continuous environment fields via implicit functions. *arXiv* preprint arXiv:2111.13997, 2021.
- [50] A. Simeonov, Y. Du, A. Tagliasacchi, J. B. Tenenbaum, A. Rodriguez, P. Agrawal, and V. Sitzmann. Neural descriptor fields: Se (3)-equivariant object representations for manipulation. arXiv preprint arXiv:2112.05124, 2021.
- [51] Y. Li, S. Li, V. Sitzmann, P. Agrawal, and A. Torralba. 3d neural scene representations for visuomotor control. In *Conference on Robot Learning*, pages 112–123. PMLR, 2022.
- [52] Z. Jiang, Y. Zhu, M. Svetlik, K. Fang, and Y. Zhu. Synergies between affordance and geometry: 6-dof grasp detection via implicit representations. *arXiv* preprint arXiv:2104.01542, 2021.
- [53] M. Adamkiewicz, T. Chen, A. Caccavale, R. Gardner, P. Culbertson, J. Bohg, and M. Schwager. Vision-only robot navigation in a neural radiance world. *IEEE Robotics and Automation Letters*, 7(2):4606–4613, 2022.
- [54] Y.-W. Chao, W. Yang, Y. Xiang, P. Molchanov, A. Handa, J. Tremblay, Y. S. Narang, K. Van Wyk, U. Iqbal, S. Birchfield, et al. Dexycb: A benchmark for capturing hand grasping of objects. In *Proceedings of the IEEE/CVF Conference on Computer Vision and Pattern Recognition*, pages 9044–9053, 2021.

- [55] K. Sohn, H. Lee, and X. Yan. Learning structured output representation using deep conditional generative models. *Advances in neural information processing systems*, 28, 2015.
- [56] C. R. Qi, H. Su, K. Mo, and L. J. Guibas. Pointnet: Deep learning on point sets for 3d classification and segmentation. In *Proceedings of the IEEE conference on computer vision and pattern recognition*, pages 652–660, 2017.
- [57] Z. Chen and H. Zhang. Learning implicit fields for generative shape modeling. In *Proceedings* of the IEEE/CVF Conference on Computer Vision and Pattern Recognition, pages 5939–5948, 2019.
- [58] B. Calli, A. Singh, A. Walsman, S. Srinivasa, P. Abbeel, and A. M. Dollar. The ycb object and model set: Towards common benchmarks for manipulation research. In *2015 international conference on advanced robotics (ICAR)*, pages 510–517. IEEE, 2015.
- [59] S. M. LaValle et al. Rapidly-exploring random trees: A new tool for path planning. 1998.
- [60] R. Rubinstein. The cross-entropy method for combinatorial and continuous optimization. *Methodology and computing in applied probability*, 1(2):127–190, 1999.
- [61] J. M. Maciejowski. Predictive control: with constraints. Pearson education, 2002.
- [62] F. Xiang, Y. Qin, K. Mo, Y. Xia, H. Zhu, F. Liu, M. Liu, H. Jiang, Y. Yuan, H. Wang, et al. Sapien: A simulated part-based interactive environment. In *Proceedings of the IEEE/CVF Conference on Computer Vision and Pattern Recognition*, pages 11097–11107, 2020.
- [63] Y. Zhou, C. Barnes, J. Lu, J. Yang, and H. Li. On the continuity of rotation representations in neural networks. In *Proceedings of the IEEE/CVF Conference on Computer Vision and Pattern Recognition*, pages 5745–5753, 2019.

A Implementation Details

Environment. Environments are built upon the Sapien [62] simulator with timestep set to 0.004 and frame skip set to 5. The action space is the motor commands of the 22 actuators on the robot's hand. The first 6 motors control the global position and orientation of the robot while the last 16 motors control the fingers of the hand. For the evaluation, we propose one manipulation task: *Lifting*. The success criteria are (i) the object and the hand are in contact and (ii) the object is lifted by 4 cm.

Network Architecture. We show our network architectures during training and testing in Tab. 4 and Tab. 5 respectively. During training, the object point cloud and 20 frames of hand joints positions are utilized as inputs. Then a PointNet encoder and a MLP encoder are employed to extract object feature \mathcal{F}^o and a set of hand features $\{\mathcal{F}^h_t\}$ respectively. Then all features are concatenated and passed to the CVAE encoder to predict the posterior distribution $\mathcal{Q}(z|\mu,\sigma^2)$. Then, a latent code z is sampled from the distribution, and concatenated with the object feature \mathcal{F}^o and query time t as the input of CGF for regressing the hand joint positions. Note that the global rotation (in the form of axis angle) is converted to the continuous 6d representation [63]. In the end, a forward kinematics layer is utilized to convert the joint positions to the Cartesian coordinates.

Stage	Configuration	Output			
0	Input object point cloud \mathcal{P}^o	2000×3			
U	Input joint positions $\{q_t\}$	20×22			
Feature extraction					
	PointNet encoder	$1024 (\mathcal{F}^o)$			
1	MLP encoder (22, 256, 256, 64)	$20 \times 64 \left(\left\{ \mathcal{F}_t^h \right\} \right)$			
Calculating distribution (Input $concat(\{\mathcal{F}_t^h\}, \mathcal{F}^o)$)					
2	CVAE encoder	256 (μ)			
	(2304, 256, 256)	$256 (\sigma^2)$			
Latent code sampling					
3	Sampling from $Q(z \mu, \sigma^2)$	256 (z)			
Hand reconstruction (Input $concat(\mathcal{F}^o, z, t)$)					
4	Continuous Grasping Function (1281, 512, 256, 25)	$25 \left(\hat{q}_t\right)$			
4	Forward Kinematics Layer	$15 \times 3 \left(\mathcal{J}_i(\hat{q}_t) \right)$			

Stage	Configuration	Output			
0	Input object point cloud \mathcal{P}^o	2000×3			
Feature extraction					
1	PointNet Encoder	$1024 (\mathcal{F}^o)$			
Latent code sampling					
3	Sampling from $\mathcal{N}(z 0,1)$	256(z)			
Hand reconstruction (Input $concat(\mathcal{F}^o, z, t)$)					
4	Continuous Grasping Function (1281, 512, 256, 25)	$25(\hat{q}_t)$			
4	Forward Kinematics Layer	$15 \times 3 \left(\mathcal{J}_i(\hat{q}_t) \right)$			

Table 5: Test-time architecture.

Table 4: Training time architecture.

During inference, the latent code z is randomly sampled from the standard Gaussian distribution $\mathcal{N}(z|0,1)$. Hence the hand joint positions and the CVAE encoder are not required.

B Ablation Study on Augmented PD Control

We perform an ablation study on augmented PD control compared with PD control. Specifically, we set the speed to 1x, 2x, and 3x, and set the mass of the robot to 1x, 2x, and 3x. We combine them in pairs and report the augmented PD control's improvement on the success rate in simulator in Tab. 6. It can be seen that the augmented PD control has improvements in all various cases, which proves its robustness.

	Mass 1x	Mass 2x	Mass 3x
Velocity 1x	5.66%	4.15%	7.10%
Velocity 2x	14.95%	7.73%	2.10%
Velocity 3x	4.29%	1.65%	16.77%

Table 6: The improvement of augmented PD control over PD control on success rate.

C Real-world Experiments on Unseen Object

Given the point cloud of unseen objects, we also sample grasping trajectories and test them in the simulator and then the real world. We visualize the successful grasping trajectories in Fig. 6, which demonstrates the generalization ability of our CGF.

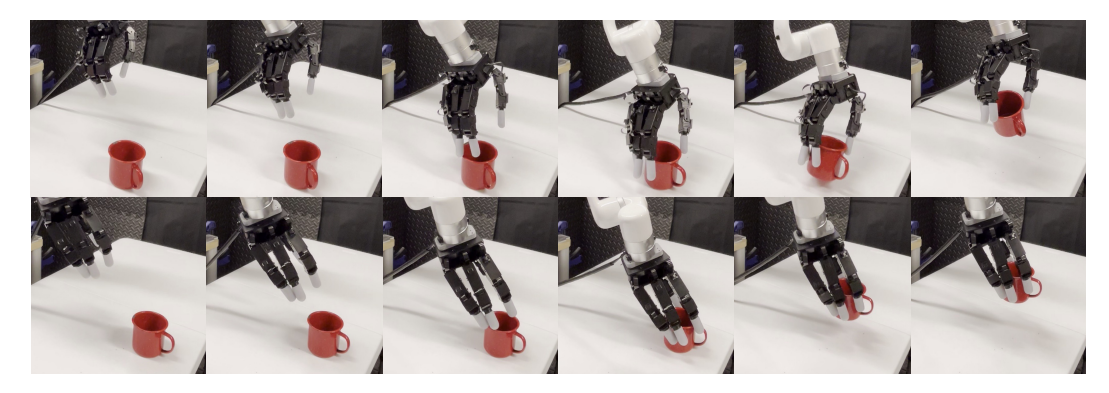


Figure 6: Real-world results on Mug. Our CGF allows generalization to manipulate unseen objects.